Published in final edited form as:
J Neural Eng. 2009 April ; 6(2): 026002. doi:10.1088/1741-2560/6/2/026002.

A Fully Implantable 96-channel Neural Data Acquisition System

Michael Rizk[1], **Chad A Bossetti**[1], **Thomas A Jochum**[1], **Stephen H Callender**[1], **Miguel A L Nicolelis**[2,3], **Dennis A Turner**[2,4], and **Patrick D Wolf**[1]

1*Department of Biomedical Engineering, Duke University, Durham, NC 27708, USA*

2*Department of Neurobiology, Duke University, Durham, NC 27710, USA*

3*Center for Neuroengineering, Duke University, Durham, NC 27710, USA*

4*Division of Neurosurgery, Duke University, Durham, NC 27710, USA*

Abstract

A fully implantable neural data acquisition system is a key component of a clinically viable brain-machine interface. This type of system must communicate with the outside world and obtain power without the use of wires that cross through the skin. We present a 96-channel fully implantable neural data acquisition system. This system performs spike detection and extraction within the body and wirelessly transmits data to an external unit. Power is supplied wirelessly through the use of inductively-coupled coils. The system was implanted acutely in sheep and successfully recorded, processed, and transmitted neural data. Bidirectional communication between the implanted system and an external unit was successful over a range of 2 m. The system is also shown to integrate well into a brain-machine interface. This demonstration of a high channel-count fully implanted neural data acquisition system is a critical step in the development of a clinically viable brain-machine interface.

1. Introduction

A brain-machine interface (BMI) provides a means of restoring motor function and communication ability to individuals suffering from nerve damage due to spinal cord injury, stroke, or neurodegenerative diseases. BMIs have already been demonstrated in a laboratory setting [1–3] and in experimental clinical settings [4–6], but in their current state they are not suitable for general clinical use. One of the major obstacles that must be overcome in order to make a BMI clinically viable is the development of fully implantable neural recording systems [7]. Fully implantable systems have no chronic through-the-skin connections and consequently minimize the risk of infection. They remove tethering issues, awkward protrusions from the body, and infection and safety concerns that are associated with percutaneous recording systems.

A fully implantable system must use wireless means to interact with the outside world. High channel-count systems generally collect more data than can be transmitted using an implantable telemetry system and, as a result, must perform data reduction in the implanted module [8–12]. Power for the implanted module must be provided by either an internal source (an implanted battery, for example) or an external source via a wireless link. In addition, such systems must deal with size and power constraints [13].

E-mail: E-mail: mr38@duke.edu.

We have developed a fully implantable 96-channel neural data acquisition system. While several neural signal processors have been developed for use in implantable systems [9–12], to the best of our knowledge, this is the first demonstration in the literature of the full implantation of a high channel-count neural data acquisition system. It should be noted, however, that low channel-count neural data acquisition systems have already been fully implanted in humans for several years [14]. Section 2 presents the overall design of the system and a description of its individual components. Section 3 presents the procedure for and results of acutely implanting our system in sheep. We show that our system is able to record, process, and wirelessly transmit neural data from inside the body. No through-the-skin connections are needed for communication or power delivery. Our goal in developing this system has been to make it suitable for use as part of a clinically viable BMI. To this end, we discuss the integration of this device into a BMI system.

2. System Design

Our neural data acquisition system is made up of both implanted components and external components. The implanted components are three digitizing headstage modules and an implantable central communications module (ICCM). The external components are a transcutaneous energy transfer system (TETS) driver circuit, a wireless communications module (WCM), and a custom-designed graphical user interface (GUI). The implanted portion of the system is powered by the TETS. This method of powering the system, along with the use of a wireless link for communication between the ICCM and the WCM, allows the system to be fully implanted, requiring no wires to cross through the skin. Figure 1 presents a block diagram of the full system.

2.1. Digitizing Headstage Modules

The digitizing headstage modules perform the first layer of processing on extracellular potentials recorded by electrodes implanted in the cortex. Each headstage records from 32 electrodes and contains two custom integrated circuits to provide amplification and filtering, two analog-to-digital converters (ADCs), and a complex programmable logic device (CPLD). Each amplifier/ADC pair amplifies, filters, and digitizes data for 16 channels. Each set of 16 channels uses its own local reference electrode. A headstage is shown in figure 2. As seen at the left of the figure, each headstage has a 36-pin, dual-row Omnetics (Minneapolis, MN) nano connector for connecting to electrode arrays. This connector allows the headstage to be reused with multiple, non-reusable electrode arrays. Alternatively, the connector can be removed and wires attached directly for permanent implantation.

The block diagram of the custom integrated circuit is shown in figure 3. The pre-amplifiers, switched-capacitor filters, and multiplexer are identical to those in an earlier integrated circuit [15]. Digital-to-analog converters (DACs) and a differential amplifier were added to the earlier circuit. The differential amplifier was tailored to mate with the high input capacitance and limited input voltage range of the ADC. The digital-to-analog converters adjust the DC level at the output of the differential amplifier to the middle of the input range of the ADC. This ensures that large extracellular potentials can be digitized without clipping the peaks of the waveforms. The digital input to the digital-to-analog converter is determined and stored during a reset sequence for the headstage.

The layout of the custom chip is presented in figure 4. The die is 4.6 mm × 4.3 mm. There are 89 pads. A standard commercial package with 89 pins would be too large for the headstage. The need for a package is eliminated by directly mounting the custom integrated circuit to the headstage using flip-chip bonding [16]. The 100 nF off-chip capacitors in the block diagram (figure 3) are soldered to the underside of the headstage and cannot be seen in figure 2.

The ADCs (AD7450A, Analog Devices, Norwood, MA) sample each channel at 31.25 kHz with 12 bits of resolution. The CPLD (XCR3064XL, Xilinx, San Jose, CA) provides timing and control signals to the amplifiers and ADCs and sends the digitized data for each set of 16 channels serially to the ICCM. Soldered to each headstage (in place of the connector at the right of figure 2) is a cable that terminates in a 12-pin circular Omnetics connector. This allows the headstage to be connected to the ICCM. Our system uses three headstages, for a total of 96 channels. Each headstage consumes approximately 0.3 W, primarily in the amplifiers.

2.2. Implantable Central Communications Module

The ICCM serves three primary functions – to regulate and provide power for all portions of the implanted system, to perform data reduction on the neural data received from the headstages, and to communicate wirelessly with the WCM. The aspects of the system related to power will be presented in section 2.3. Data processing in the ICCM is performed in a field programmable gate array (FPGA). A full description of the processing performed in this FPGA (Xilinx Virtex-II XC2V1000) can be found in [12]. Data reduction is performed by applying a threshold to the absolute value of the data on each channel. When a threshold is crossed, a spike waveform is extracted and stored along with a timestamp and the number of the channel on which the spike occurred. Every 50 ms, the extracted spikes are transmitted wirelessly out of the ICCM. Other data output modes are available as well, including sending out 1-ms bin counts for all 96 channels or all samples recorded on a single channel (i.e., full streaming data for a single channel) along with the extracted spikes for that channel.

The wireless communication is bidirectional. This allows the ICCM to not only send neural data out of the body but also to receive commands and configuration information from the WCM. Telemetry is performed using a commercial one-megabit-per-second transceiver (TR1100, RF Monolithics, Inc., Dallas, TX). This transceiver operates at 916.5 MHz. The system can operate in Loopback mode in order to test telemetry performance. In this mode, the WCM sends a packet of 256 bytes to the ICCM every 50 ms. The ICCM responds by echoing back the data that it has received.

Figure 5 shows an ICCM board. Five cables must be soldered onto this board to allow for interaction with the other components of the system. Three cables terminate in circular Omnetics connectors to allow for the three headstages to plug into the ICCM. One cable connects an antenna to the ICCM to allow for wireless communication with the WCM, and one cable connects the TETS secondary coil (section 2.3) to the ICCM. Including losses present in the regulators (see section 2.3), the ICCM consumes approximately 1 W.

2.3. Transcutaneous Energy Transfer System

The concept of using inductively-coupled coils to power implanted medical devices has been demonstrated in a number of well-known applications [10,17–21]. For our application, a TETS was designed to provide the roughly 2 W required by the 96-channel system. The complete circuit topology for the TETS is shown in figure 6. The TETS design uses a novel technique for mitigating coil misalignment, employing high input-voltage step-down switching regulators in the secondary. The primary coil driver, coils, and rectifying stage were designed to significantly exceed the minimum input voltage (dropout voltage) of the regulators. As the coils become misaligned, the excess voltage serves as a buffer to keep the system in regulation. Switching regulators are used for this approach because they remain efficient for input voltages well above their dropout voltages. The remainder of this section outlines the major subcircuits that implement this approach.

Unlike many TETS designs that use a class-E primary driver, a 250-kHz H-bridge inverter was used in this design. An H-bridge converts DC to AC by switching on anti- parallel pairs of

MOSFETs. This switching regime presents a square wave of voltage to the primary coil. The voltage waveform is integrated by the inductor, producing a triangle wave of current. This subcircuit consists of a HIP4080A (Intersil, Milpitas, CA) full-bridge switcher, four IRFR4105 power MOSFETs (International Rectifier, El Segundo, CA), and a 24-V DC power source. A hot swap electronic circuit breaker is also employed in this circuit (not shown in the figure), to provide undervoltage, overvoltage, and short circuit protections. To house all of the components of the primary, a 6-layer, 7 cm × 10 cm circuit board was designed and fabricated.

The primary and secondary coils were custom wound from litz wire. The primary coil had an inner diameter of 30 mm and an outer diameter of 56 mm. The secondary coil had an inner diameter of 30 mm and an outer diameter of 45 mm. In the context of this application, the primary coil is placed outside of the body and the secondary coil is implanted inside the body.

Referring again to the topology shown in figure 6, following the secondary coil, the first stage of the secondary circuit is a voltage doubler rectifier. This stage then feeds a pair of LT1766 switching regulators (Linear Technology, Milpitas, CA), which can tolerate input voltages as high as 60 V and can source as much as 1.5 A. The switching regulators feed a combination of linear regulators (Linear Technology). These final regulators provide low-noise power to the sensitive digital and analog devices within the acquisition system. Also included in the secondary are two bulk DC storage capacitors, for additional system holdup. If the coils become completely separated, these 470 μF capacitors allow the system to continue to operate for approximately 66 ms. All of the components of the secondary circuit are located on the ICCM.

Once all of the components of the complete 96-channel system were fully built and individually tested, the complete system was powered by the TETS and tested on the lab bench. The secondary coil was immersed in a 0.9% saline bath (an approximation of the conductivity of blood). The two coils were displaced both axially and radially, while voltage and current were monitored in the secondary. The system was able to maintain regulation with the two coils axially separated by up to 2 cm, with perfect radial alignment. Alternatively, with a fixed axial separation of 1.5 cm, the system was able to tolerate a radial displacement of approximately 1.5 cm. Overall DC-to-DC efficiency was 24.6%.

2.4. Wireless Communications Module

The WCM's primary function is to communicate with the ICCM. The WCM relays commands to and receives data from the ICCM. This data can then be passed on for use elsewhere. A board identical to that used for the ICCM (see figure 5) is used for the WCM. Since the ICCM and WCM must perform different processing tasks, the FPGAs on the two boards are programmed differently. We have developed a LabView graphical user interface to serve as a link between a user and the WCM. The WCM interfaces to a digital I/O data acquisition card (NI 653X, National Instruments, Austin, TX) installed in the computer running the user interface. A user can view and store data output from the WCM through this interface. This user interface also provides a means by which commands and configuration information can be sent to the WCM and ultimately to the ICCM.

The WCM, in some cases, can perform further processing on the data that it receives from the ICCM. The WCM has the capability of compiling 1-ms bin counts received from the ICCM into 50-ms bin counts and outputting these more commonly used variables. Our system is also able to perform spike sorting using a two-phase process. Spike templates are generated during a learning phase and then template matching is performed in a real-time phase. In the first phase of spike sorting, the WCM outputs extracted spike waveforms that it receives from the ICCM. These spikes are passed on to commercial spike sorting software (Offline Sorter, Plexon Inc., Dallas, TX) by means of the user interface. The user interface writes the extracted spikes to a file in Plexon's .plx format. A user then utilizes the features of the spike sorting software to

generate up to four templates per channel based on the extracted waveforms. These templates are then saved in Plexon's .tpl file format and uploaded to memory in the WCM's FPGA. During the real-time template-matching phase, the ICCM continues to detect and extract spikes and send them to the WCM. As the WCM receives extracted spikes, it compares the received spike with the templates that were generated from the spikes found on the corresponding channel during the template-generating phase. The sum of squared errors between the extracted spike and each of the applicable templates is computed. Each template is also shifted one and two samples (32 μs per sample) in each direction in order to reduce errors due to alignment issues. A spike is classified as matching the template that either in its original form or a shifted form results in the minimum sum of squared errors, as long as the computed sum of squared errors is below a specified value. Based on these classifications, the WCM generates 50-ms bin counts for each template. These 384 bin counts (4 *templates/channel* * 96 *channels* = 384 *templates*) are sent out of the WCM every 50 ms. Additionally, the option exists to output each individual extracted waveform along with its classification category and an indication of the amount of template shifting that was found to be optimal.

2.5. Percutaneous Live Animal Recordings

Once the entire system was designed, built, and tested on the bench, we recorded from an owl monkey with percutaneous electrodes implanted in its cortex. During these recordings, the entire pathway for the flow of neural information (from the headstages to the ICCM to the WCM to the user interface) was in use. Figure 7 shows examples of neural data recorded from the owl monkey. For these particular recordings, the ICCM was powered by a rechargeable battery rather than the TETS.

2.6. Electrodes and Packaging for Implantation

Prior to implantation, the entire system was packaged for operation inside the body. Electrode arrays were hand-assembled using 30-μm and 50-μm diameter tungsten wires. Electrode shanks were 2 mm, 2.5 mm, and 3 mm long and were spaced 300 μm to 500 μm on center. The electrodes were insulated with polyimide, which was removed at the tips when the electrodes were clipped to length. The tungsten wires extended 2.5 cm to 3.5 cm back from the electrode tips and terminated into a small printed wire board to which an Omnetics connector was attached. This allowed the array to be plugged into a headstage.

The electronic components of each headstage were coated with a layer of Loctite Hysol epoxy (Henkel, Dusseldorf, Germany). The electrodes were then attached, and a fine layer of flowable silicone adhesive (Permatex, Hartford, CT) was poured over the epoxy layer and electrode connector. The outer sheath of all cables extending from the headstages and the ICCM was medical grade silicone tubing. This tubing was sealed at the ends with silicone adhesive.

Low-profile ceramic magnets were fixed in the center of the primary and secondary TETS coils. These magnets were used to hold the coils in proximity during acute animal studies. The use of ceramics mitigated power loss from eddy currents. A braided ground sheath was threaded over the leads of both coils. For the secondary, medical grade silicone tubing was threaded over the ground sheath, up to the base of the coil. The coil was then encapsulated with A-103, MDX4-4210 platinum cure silicone elastomer (Factor II, Lakeside, AZ).

After all subassemblies and cables were encapsulated, the ICCM was packaged in a titanium can. Several holes were first drilled in the can for cable egress. The surface of the can was prepared before applying sealant. This process included abrasion, cleaning, and treatment with MED-163 silicone primer (Nusil, Carpinteria, CA), to increase the effectiveness of the silicone adhesive. With the ICCM inside and cables appropriately routed, clear RTV silicone adhesive sealant (Permatex) was applied over the seam, in sections. Between sections, the adhesive was

cured at 60°C. The final section, which completed sealing the can, was applied at room temperature to prevent inward pressure during *in vivo* operation. A final thin coat of flowable silicone adhesive was applied over the sealant to fill small seams and voids. A photograph of the packaged system is presented in figure 8.

With the implanted components fully sealed, the acquisition system was tested in a 0.9% saline bath. All components were completely submerged for a period of no less than three hours. The headstage-to-ICCM connectors were left out of the bath, since they remain unsealed until implant. The secondary coil was mounted against the inside of the bath's plastic wall, below the water line. The primary coil was mounted opposite the secondary coil, on the exterior of the bath. With this configuration, the system could be powered throughout testing.

The performance of the acquisition system was informally evaluated by monitoring its ability to acquire and telemeter an injected test signal. The signal was induced in the bath using two electrodes and a signal generator. These signals provided verification of the system's functionality.

In instances in which a minor compromise in the packaging was discovered, repairs were made by applying additional silicone adhesive. On some occasions, major leaks were detected in the ICCM enclosure sealant. Repairs were made by completely disassembling the enclosure, cleaning off the original layer of sealant, and repeating the process described above. Since saline was used in the bath, whenever a leak occurred, the ICCM electronics were usually damaged in some way. In all cases, appropriate repairs were made and all system components were fully re-tested before resealing the enclosure.

3. Performance of the Fully Implanted System

3.1. Surgical Procedure

Our system was implanted acutely in six sheep. The purpose of these experiments was twofold – 1) to develop the implantation procedures and 2) to test the system functionally in a controlled environment. All implantation procedures were performed in accordance with a protocol approved by the Duke University Institutional Animal Care and Use Committee. While the exact surgical procedure varied slightly from animal to animal, the general procedure was as follows. The animal was anesthetized with isofluorane to initially maintain sedation/analgesia, but then switched over (after ~1 hour) to a combination of propofol and narcotics to permit continued breathing and to allow cortical stimulation and recording (which is not possible under inhalation anesthesia). A midline scalp incision was made anterior to the brow, between the horns and orbital rims, to gain enough anterior exposure to the motor strip along the midline. We performed a right-sided craniotomy from across the midline on the left to far laterally on the right, almost to the horn protuberance, and anteriorly to between the orbital rims. This craniotomy was ~1.5 cm (lateral) × 3 cm (anterior-posterior), based posteriorly on the lambdoid suture. Anteriorly the outer cortex of the skull overlays the large frontal air sinus, so after drilling through the outer skull, the mucosa was pulled out of the sinus to help prevent bleeding. Then, the interior of the sinus was drilled down to expose the dura. The dura was opened laterally and then taken medially to the midline at both the anterior and posterior aspects of the incision. The arachnoid was kept intact if possible and opened selectively over a sulcus to specifically expose the pia. A World Precision Instruments (Sarasota, FL) constant-current stimulator unit was used to perform cortical stimulation. After confirming that muscle tissues were excitable following the anesthesia switch, bipolar tips were used with 60 Hz, 10 mA stimulation to attempt to identify the motor cortex. We reliably found a large area for face and smaller areas for forelimb and hindlimb, on the medial gyrus noted to be motor cortex in atlases. We then inserted the three electrode arrays into the cortex while recording directly from the headstages. Once the arrays were in place, the electrode cables (i.e., the tungsten wires running

from the implanted arrays to the headstages) and the headstages were secured to the skull with small screw-down clamps. The bone flap was then secured in place.

The ICCM was implanted in a muscular pocket in the upper chest or neck region. Cables were tunneled underneath the skin from the headstages (which lay on top of the skull) to the ICCM. Once the headstages and ICCM were connected, MED2-4213 silicone adhesive (Nusil) was used to backfill silicone boots that extended over each pair of connectors. The silicone adhesive was cured using a heat gun. The TETS secondary coil and the implantable antenna were tunneled caudally and dorsally, respectively, away from the ICCM. Once the full system was implanted, all openings in the skin were closed with sutures.

3.2. Neural Data

Figure 9 shows a sample of neural data recorded using the fully implanted system. As seen in the figure, the noise floor is low enough that spikes are clearly discernible. The root-mean-square value for the entire waveform shown in figure 9(a) (including the spikes) is 7 μV. It must be emphasized that these recordings were made with a fully implanted system being powered wirelessly and sending data out of the body wirelessly. All aspects of our system were able to operate without significantly corrupting the neural data.

Figure 10 shows spikes extracted by our system from selected channels over a roughly one-minute period of recording. The system was in the "extracted spikes mode" and was attempting to extract spikes from all 96 channels simultaneously. Only a subset of the 96 channels actually had spikes on them.

In figure 9 and figure 10, both positive-going and negative-going spikes are visible. Our system performs differential recordings. Each set of 16 channels has a local reference electrode. If an active neuron is located near the reference electrode, inverted (i.e., positive-going) spikes will appear on each channel that uses that reference electrode. Figure 9(b) presents an example of a recording that appears to contain spikes both from a neuron near the particular channel's electrode and from a neuron near the reference electrode. The suspicion of the presence of a neuron near the reference electrode was supported in this case by looking at the spikes extracted by the ICCM. We found that a significant proportion of the extracted spikes on the set of 16 channels (see figure 10) had identical timestamps on all 16 channels. It is extremely unlikely that this would have been observed based on the activity of individual neurons located near each of the 16 individual electrodes.

3.3. Telemetry

We tested the telemetry performance of our system while the system was fully implanted. This was done using our system's Loopback mode. Table 1 shows the results for several different circumstances. These circumstances use various combinations of implanted ICCM antennas, distances between the ICCM and WCM antennas, and relative orientations between the antennas. In each case, the WCM antenna was a commercial half-wavelength dipole (ANT-916-MHW-RPS-S, Antenna Factor, Merlin, OR). We used two different designs for the subcutaneous ICCM antenna – a dipole made of flexible, stranded stainless steel wire and a monopole made by stripping off the appropriate length of shielding from a coaxial cable. The monopole and each leg of the dipole were 4 cm long. For each circumstance, the table presents the number of packets that the WCM received back from the ICCM as well as the number of packets that were dropped. A "dropped" packet occurs when the WCM sends out the Loopback command but does not receive any packet from the ICCM in response. We also list the number of received packets that contained errors. These results are not meant to be a comprehensive evaluation of the telemetry performance of the implanted system. Rather, they give a general idea of the level of performance under different circumstances.

4. Discussion

4.1. System Components

The two custom integrated circuits on the headstage are the only electronics in the implantable system that are not built from readily-available and well-proven components. Thirty-two commercial amplifiers would not fit on the headstage, so custom circuitry was unavoidable. The design of the custom circuitry followed the low-risk path of classic CMOS analog techniques. The benefit of this decision was that the progress of the entire implanted system was never jeopardized by redesign of the custom integrated circuit. The drawback was that the resulting circuits use more power, more area, and more off-chip components than recent innovative circuits [22,23].

Section 2.4 stated that the real-time template-matching phase of the spike sorting process is performed in the WCM. An alternative location for performing template matching could be the ICCM's neural signal processor. Rather than sending extracted spikes out of the body and performing template matching in the external processor, we could extract the spikes and perform the template matching inside the body. Then, for example, sorted bin counts could be sent out of the body. This would be advantageous because it would significantly decrease the burden on the telemetry system. We have not implemented template matching in this manner simply because the ICCM's FPGA does not have enough resources to perform template matching in addition to all of its current functions. Nevertheless, the potential for performing template matching within the body exists if the ICCM were to use an FPGA with more resources or if we were to remove some of the functionality of the current neural signal processor.

An advantageous feature of our system is the power delivery capability of the TETS. As cited in section 2.3, there are many examples in the literature of both low-power (<100 mW) and high-power (≥10 W) TETS designs. Conspicuously absent from the literature is a mid-range TETS solution for providing approximately 1–3 W to an implanted medical device. What is advantageous about this power range is that it introduces the possibility of using the TETS in future battery-charging applications. Powering a continuously operating, chronically implanted system from a primary cell is not feasible for systems that consume even moderate power. An alternative is to use an implanted rechargeable battery. If powered by a rechargeable battery, an implanted neural data acquisition system capable of transmitting data a distance of 1–2 m would allow a patient to be completely free of external components except when recharging the battery.

4.2. Power Consumption and Temperature

A major consideration in the design of the 96-channel system has been whether 2 W is an excessive power dissipation for an implanted system [24]. The Food and Drug Administration (FDA) regulates the medical device industry through consensus standards. One such standard requires that the outer surface of any part of an implantable device should not exceed 2°C above the normal body temperature of 37°C as a result of normal operation or any single fault condition [25]. A series of in-depth studies investigated the relationship between device power consumption and temperature rise in tissue [26–30]. These studies presented key findings concerning how tissue responds to temperature rise and provided experimental data that established a link between power consumption and surface temperature increases. For muscle, the results indicated that power densities of 60 mW/cm^2 and 80 mW/cm^2 increased the baseline tissue temperature by 4–7°C, while a power density of 40 mW/cm^2 limited the tissue temperature increase to 2–3°C. These data points provide insight into how to select an appropriately sized enclosure based on expected device power consumption.

The system designed during our research benefits from having its components distributed throughout the body, since this decreases the overall power density. No electrical components are in direct contact with brain tissue [31]. This relaxes some of the size and power constraints for the system. (See [23] for some of the advantages and disadvantages of this distributed architecture as compared with other architectures.) For the implanted components of the system, the power densities are approximately as follows: 32 mW/cm^2 for a single headstage; 10 mW/cm^2 for the ICCM; and less than 5 mW/cm^2 for the secondary coil. These power densities are less than 40 mW/cm^2, but the headstage is precariously close to this recommended limit. To monitor temperature rise during a chronic implant, a small 6-channel digital thermometer has been designed to fit within the titanium enclosure and connect to the ICCM. This temperature system allows bead thermistors to be positioned at the surface of any implanted component. Temperature data is passed to the ICCM and can be transmitted to the WCM. Thus, in future studies, temperature can be monitored in real-time in an ambulatory test subject.

We recognize that the power consumption of our system is far from ideal. As we have already mentioned, the amplifiers are responsible for a significant amount of our system's power consumption and newer amplifiers that consume considerably less power are feasible. Therefore, the most obvious approach to reducing our system's power consumption is to redesign the amplifiers. This redesign would also result in less wasted power in the regulation stage and might allow some regulators to be eliminated.

4.3. Telemetry

Section 3.3 presented data regarding the telemetry performance of the fully implanted system. We found that telemetry can be performed successfully over a range of a couple meters. A range on this order allows the external unit (and any equipment connected to it) to remain a reasonable distance from the implanted subject.

It should be pointed out that in all of our telemetry tests, both antennas were stationary. For a system that is implanted in a living, moving animal or person, the effect of motion between the implanted portion of the system and the external portion of the system could prove to have a significant impact on telemetry performance. As stated earlier, we did not set out to perform a comprehensive evaluation of telemetry performance for the implanted system. Rather, we have shown that our implanted system can successfully communicate with an external module over a reasonable range. Telemetry is one area in which the environment and circumstances in which the system will be used will considerably affect performance.

4.4. Acute Versus Chronic Implants

Our system has performed successfully in acute studies. The distinction between acute and chronic implants is important. The results presented in section 3 involved having our system fully implanted for several hours – not days, weeks, or months. While packaging our system for acute studies proved to be quite a challenge, robust packaging is even more critical in chronic studies.

Also, during our acute studies, the animals were anesthetized throughout the entire study. While the full system was implanted and operational during these studies, we never observed discernible neural activity on more than a small fraction of the channels. We suspect that this was in part due to the anesthesia and the acute nature of the study. A chronic implant would likely provide greater opportunities to observe neural data on a large number of channels.

Our selection of sheep for these studies was made with an eye toward performing a chronic implant. Sheep are, in addition to being large enough for our system, relatively docile animals.

With all of the challenges that will accompany an initial chronic implant, having a docile animal will be an advantage.

4.5. Physical Size of a BMI

The application that has motivated our work on a fully implantable neural data acquisition system is a BMI. BMIs that have been demonstrated so far are generally quite large. They typically utilize a large rack of signal processing hardware and computers. Our neural data acquisition system makes a reasonably sized BMI possible. A full BMI would consist of the implantable portion of our system (shown in figure 8), the external portion of our system (shown in figure 11), and a decoding application to map the acquired neural data to a control signal for a machine. Since the decoding application can run on the laptop computer that interfaces with the WCM, the components pictured in figure 8 and figure 11 represent a full BMI.

We have demonstrated the integration of our system into a BMI application using a benchtop BMI setup. The flow of information through this setup is shown in figure 12. The complete setup consists of a neural signal simulator, our neural data acquisition system, and a decoder application. The simulated neural signals encode directional information in their firing rates. The directional information is obtained from either a predetermined trajectory or through real-time control by means of a "joystick." The neural data acquisition system outputs 50-ms bin counts. The decoder application uses these bin counts to reconstruct the trajectory in real time.

The top left and bottom left of figure 12 show a predetermined trajectory and its reconstruction based on a total of 36 simulated neurons across 15 channels. The bottom right of figure 12 shows the real-time estimation of a trajectory controlled by the joystick. Fifteen channels, each with a single simulated neuron, were used in this case. Note that fairly good control of the estimated trajectory was achieved using the joystick as indicated by our ability to write "duke." It must be stated that the position of the joystick does not directly control the estimated trajectory. Rather, the position of the joystick contains information that is encoded into the firing rates of the waveforms used as input for our system. The estimated trajectory visible in the figure is the result of decoding 50-ms bin counts output by our system.

4.6. Other Uses of a Fully Implantable Neural Data Acquisition System

While the target application for our system is a BMI, a high channel-count fully implantable system can also be beneficial in other tasks. Significant effort is required in order to make wired recording systems suitable for recording from freely behaving animals [32]. Wireless recording systems that are not fully implantable have been developed in order to overcome some of the obstacles present in recording from freely behaving animals [33,34]. These systems may be suitable in some cases; however, it is likely that a fully implantable system with a significant telemetry range would be preferable in other circumstances.

Acknowledgments

The authors would like to thank E. Dixon-Tulloch for her help with the sheep studies; M. Lebedev and J. O'Doherty for their help with monkey recordings; I. Obeid for his work on an earlier wireless neural recording system that formed the foundation for this system; J. Morizio, D. Won, and H. Arora for their work on integrated-circuit design; and D. Bastakoty for his work on the interface to the spike sorting software. This work was supported by DARPA Contract Number N66001-02-C-8022, Grant Number F31EB007897 from the National Institute of Biomedical Imaging and Bioengineering, and the McChesney Foundation.

References

1. Serruya MD, Hatsopoulos NG, Paninski L, Fellows MR, Donoghue JP. Instant neural control of a movement signal. Nature 2002 Mar;416(6877):141–142. [PubMed: 11894084]

2. Taylor DM, Tillery SI, Schwartz AB. Direct cortical control of 3d neuroprosthetic devices. Science 2002 Jun;296(5574):1829–1832. [PubMed: 12052948]
3. Carmena JM, Lebedev MA, Crist RE, O'Doherty JE, Santucci DM, Dimitrov DF, Patil PG, Henriquez CS, Nicolelis MA. Learning to control a brain-machine interface for reaching and grasping by primates. PLoS Biol 2003 Nov;1(2):193–208.
4. Kennedy PR, Bakay RAE, Moore MM, Adams K, Goldwaithe J. Direct control of a computer from the human central nervous system. IEEE Trans Rehabil Eng 2000 Jun;8(2):198–202. [PubMed: 10896186]
5. Patil PG, Carmena JM, Nicolelis MAL, Turner DA. Ensemble recordings of human subcortical neurons as a source of motor control signals for a brain-machine interface. Neurosurgery 2004 Jul;55(1):27–38. [PubMed: 15214971]
6. Hochberg LR, Serruya MD, Friehs GM, Mukand JA, Saleh M, Caplan AH, Branner A, Chen D, Penn RD, Donoghue JP. Neuronal ensemble control of prosthetic devices by a human with tetraplegia. Nature 2006 Jul;442(7099):164–171. [PubMed: 16838014]
7. Lebedev MA, Nicolelis MA. Brain-machine interfaces: past, present and future. Trends Neurosci 2006 Sep;29(9):536–546. [PubMed: 16859758]
8. Bossetti CA, Carmena JM, Nicolelis MAL, Wolf PD. Transmission latencies in a telemetry-linked brain-machine interface. IEEE Trans Biomed Eng 2004 Jun;51(6):919–924. [PubMed: 15188859]
9. Olsson RH III, Wise KD. A three-dimensional neural recording microsystem with implantable data compression circuitry. IEEE J Solid-State Circuits 2005 Dec;40(12):2796–2804.
10. Harrison RR, Watkins PT, Kier RJ, Lovejoy RO, Black DJ, Greger B, Solzbacher F. A low-power integrated circuit for a wireless 100-electrode neural recording system. IEEE J Solid-State Circuits 2007 Jan;42(1):123–133.
11. Sodagar AM, Wise KD, Najafi K. A fully integrated mixed-signal neural processor for implantable multichannel cortical recording. IEEE Trans Biomed Eng 2007;54(6):1075–1088. [PubMed: 17554826]
12. Rizk M, Obeid I, Callender SH, Wolf PD. A single-chip signal processing and telemetry engine for an implantable 96-channel neural data acquisition system. J Neural Eng 2007 Sep;4(3):309–321. [PubMed: 17873433]
13. Harrison RR. The design of integrated circuits to observe brain activity. Proc IEEE 2008 Jul;96(7):1203–1216.
14. Bartels J, Andreasen D, Ehirim P, Mao H, Seibert S, Wright EJ, Kennedy P. Neurotrophic electrode: method of assembly and implantation into human motor speech cortex. J Neurosci Methods 2008 Sep;174(2):168–176. [PubMed: 18672003]
15. Morizio J, Won D, Obeid I, Bossetti C, Nicolelis MA, Wolf PD. 16-channel neural pre-conditioning device. Proc 1st IEEE EMBS Conf Neural Eng 2003:104–107.
16. Pascual DN, Callender S. Flip chip bonding: flexible circuit devices designed for biomedical applications. Adv Packag 2004 Oct;13(10):18–22.
17. Zierhofer CM, Hochmair ES. Geometric approach for coupling enhancment of magnetically coupled coils. IEEE Trans Biomed Eng 1996 Jul;43(7):708–714. [PubMed: 9216142]
18. Loeb GE, Peck RA, Moore WH, Hood K. Bion system for distributed neural prosthetic interfaces. Med Eng Phy 2001 Jan;23(1):9–18.
19. Puers R, Vandevoorde G. Recent progress on transcutaneous energy transfer for total artifical heart systems. Artif Organs 2001;25(5):400–405. [PubMed: 11403672]
20. Vandevoorde G, Puers R. Wireless energy transfer for stand-alone systems: a comparison between low and high power applicability. Sens Actuators, A 2001;92:305–311.
21. Lenaerts B, Puers R. An inductive power link for a wireless endoscope. Biosens Bioelectron 2007 Feb;22(7):1390–1395. [PubMed: 16904885]
22. Harrison RR, Charles C. A low-power low-noise cmos amplifier for neural recording applications. IEEE J Solid-State Circuits 2003 Jun;38(6):958–965.
23. Jochum T, Denison T, Wolf P. Integrated circuit amplifiers for multi-electrode intracortical recording. J Neural Eng 2009 Feb;6(1)012001

24. Wolf, PD. Thermal considerations for the design of an implanted cortical brain-machine interface (BMI). In: Reichert, WM., editor. Indwelling Neural Implants: Strategies for Contending with the In Vivo Environment. Boca Raton: CRC Press; 2008.
25. International Organization for Standardization. Implants for surgery - active implantable medical devices - part 1: general requirements for safety, marking, and for information to be provided by the manufacturer. 2000ISO 14708-1
26. Saidel GM, Davies CR, Liu EH, Harasaki H. Temperature and perfusion responses of muscle and lung tissue during chronic heating in vivo. Med Biol Eng Comput 2001 Jan;39(1):126–133. [PubMed: 11214264]
27. Davies CR, Fukumura F, Fukamachi K, Muramoto K, Himley SC, Massiello A, Chen J, Harasaki H. Adaptation of tissue to a chronic heat load. ASAIO J 1994 Jul–Sep;40(3):M514–M517. [PubMed: 8555569]
28. Liu EH, Saidel GM, Harasaki H. Model analysis of tissue response to transient and chronic heating. Ann Biomed Eng 2003 Nov;31(8):814–820.
29. Seese TM, Harasaki H, Saidel GM, Davies CR. Characterization of tissue morphology, angiogenesis, and temperature in the adaptive response of muscle tissue to chronic heating. Lab Invest 1998 Dec; 78(12):1553–1562. [PubMed: 9881955]
30. Okazaki Y, Davies CR, Matsuyoshi T, Fukamachi K, Wika KE, Harasaki H. Heat from an implanted power source is mainly dissipated by blood perfusion. ASAIO J 1997 Sep–Oct;43(5):M585–M588. [PubMed: 9360112]
31. Kim S, Tathireddy P, Normann RA, Solzbacher F. Thermal impact of an active 3-d microelectrode array implanted in the brain. IEEE Trans Neural Syst Rehabil Eng 2007 Dec;15(4):493–501. [PubMed: 18198706]
32. Eliades SJ, Wang X. Chronic multi-electrode neural recording in free-roaming monkeys. J Neurosci Methods 2008 Jul;172(2):201–214. [PubMed: 18572250]
33. Obeid I, Nicolelis MAL, Wolf PD. A multichannel telemetry system for single unit neural recordings. J Neurosci Methods 2004 Feb;133:33–38. [PubMed: 14757342]
34. Mavoori J, Jackson A, Diorio C, Fetz E. An autonomous implantable computer for neural recording and stimulation in unrestrained primates. J Neurosci Methods 2005 Oct;148:71–77. [PubMed: 16102841]

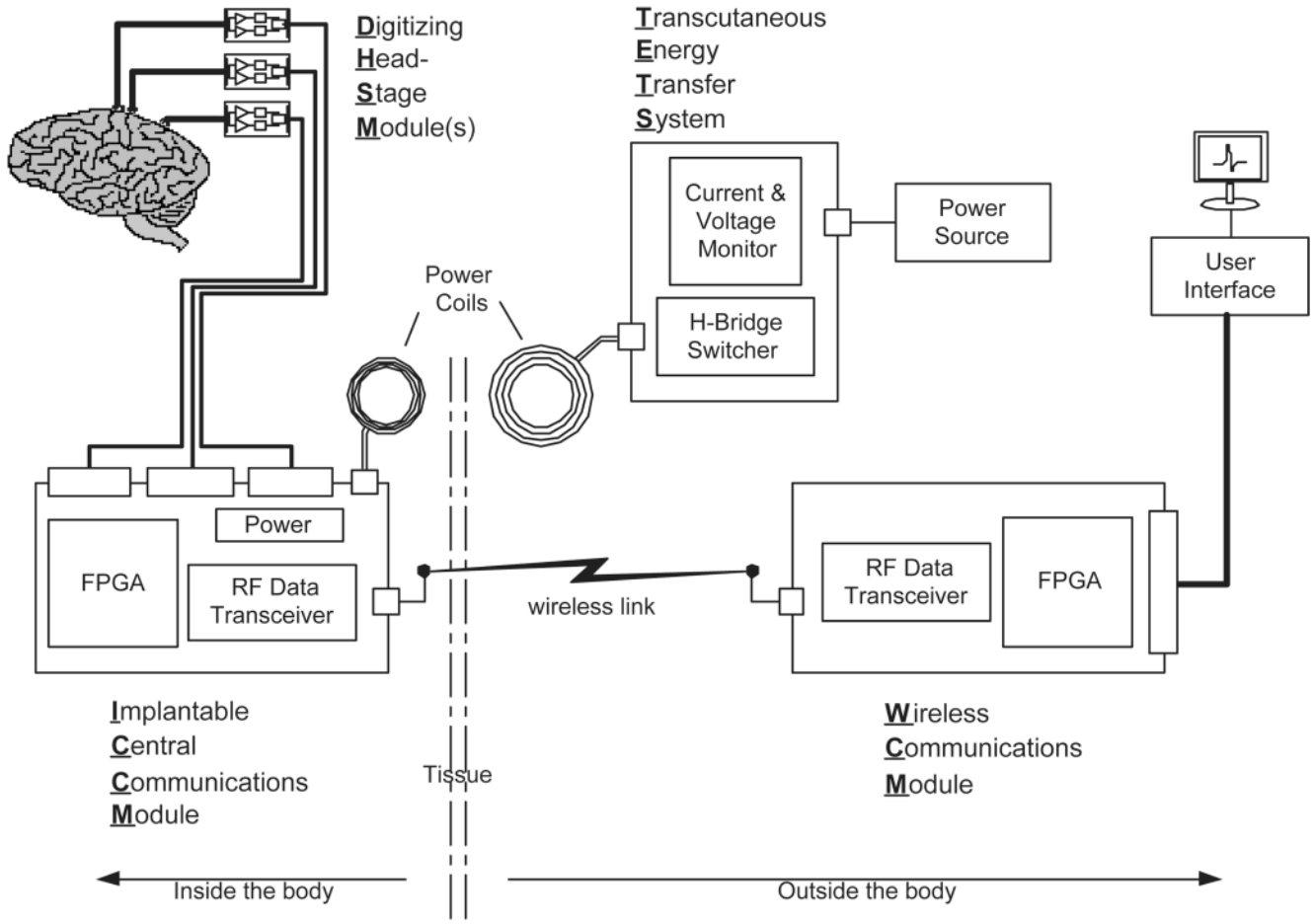

Figure 1.
Block diagram of the neural data acquisition system. Figure adapted with permission from [12].

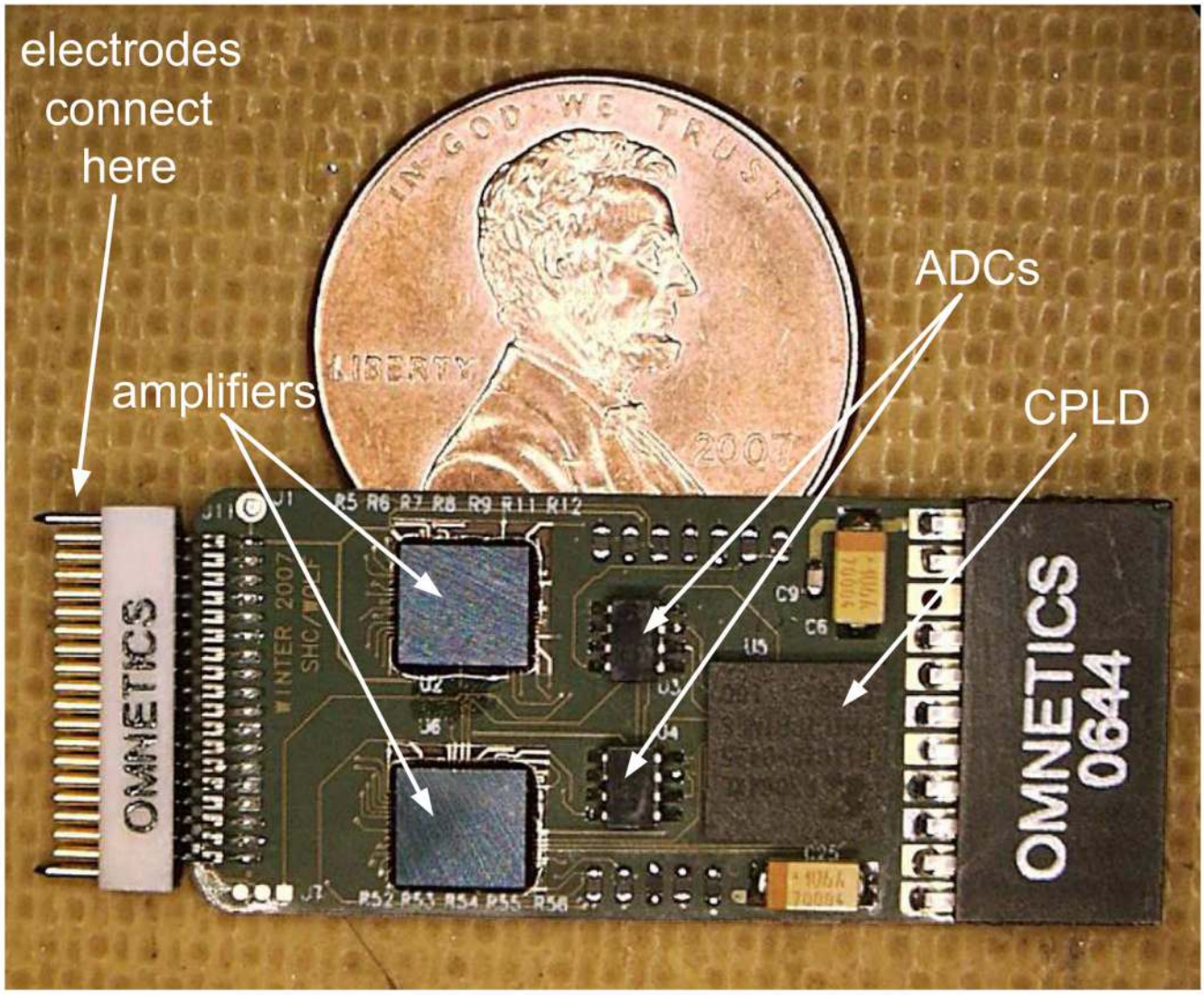

Figure 2.
The digitizing headstage module circuit board. This board contains two custom integrated circuits (each responsible for amplifying 16 channels), two analog-to-digital converters (ADCs), and a complex programmable logic device (CPLD). Neural signals picked up by the electrodes are amplified, filtered, and digitized before being passed on to the implantable central communications module (ICCM) for further processing. The connector on the right side of the figure is optional.

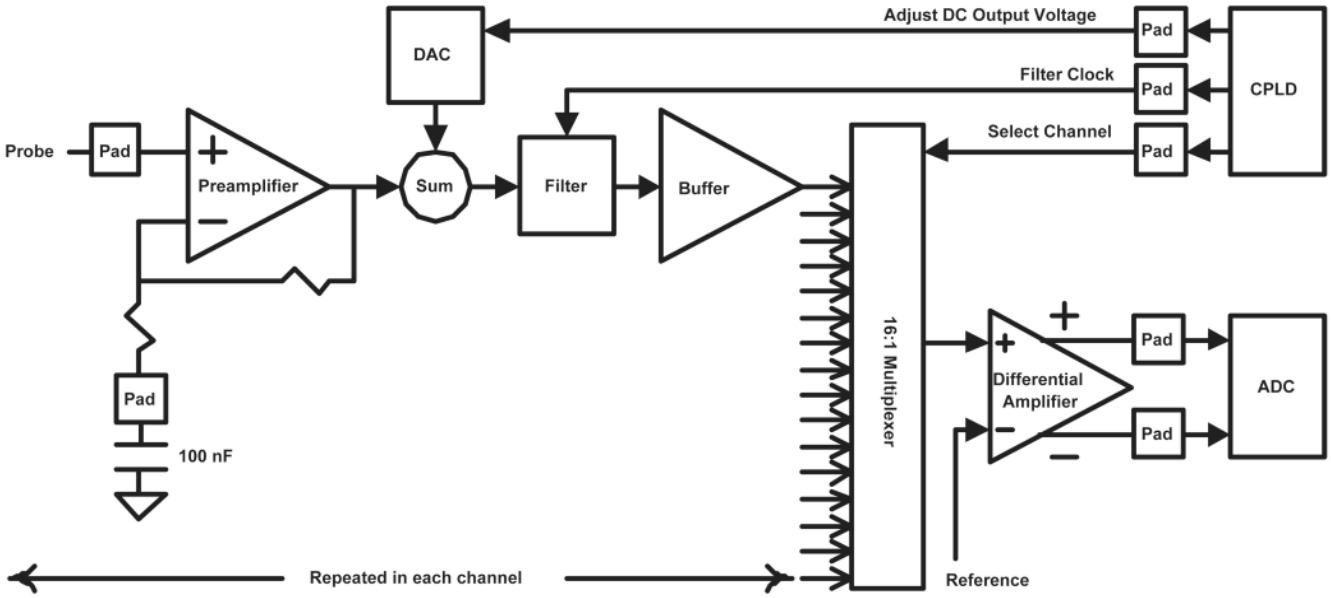

Figure 3.

Block diagram of the custom integrated-circuit amplifiers. The extracellular potential sensed by the probe is amplified to a magnitude appropriate for the ADC. Signals outside the frequency band of extracellular potentials are removed by a switched-capacitor filter. The multiplexer directs a different channel to the ADC every two microseconds.

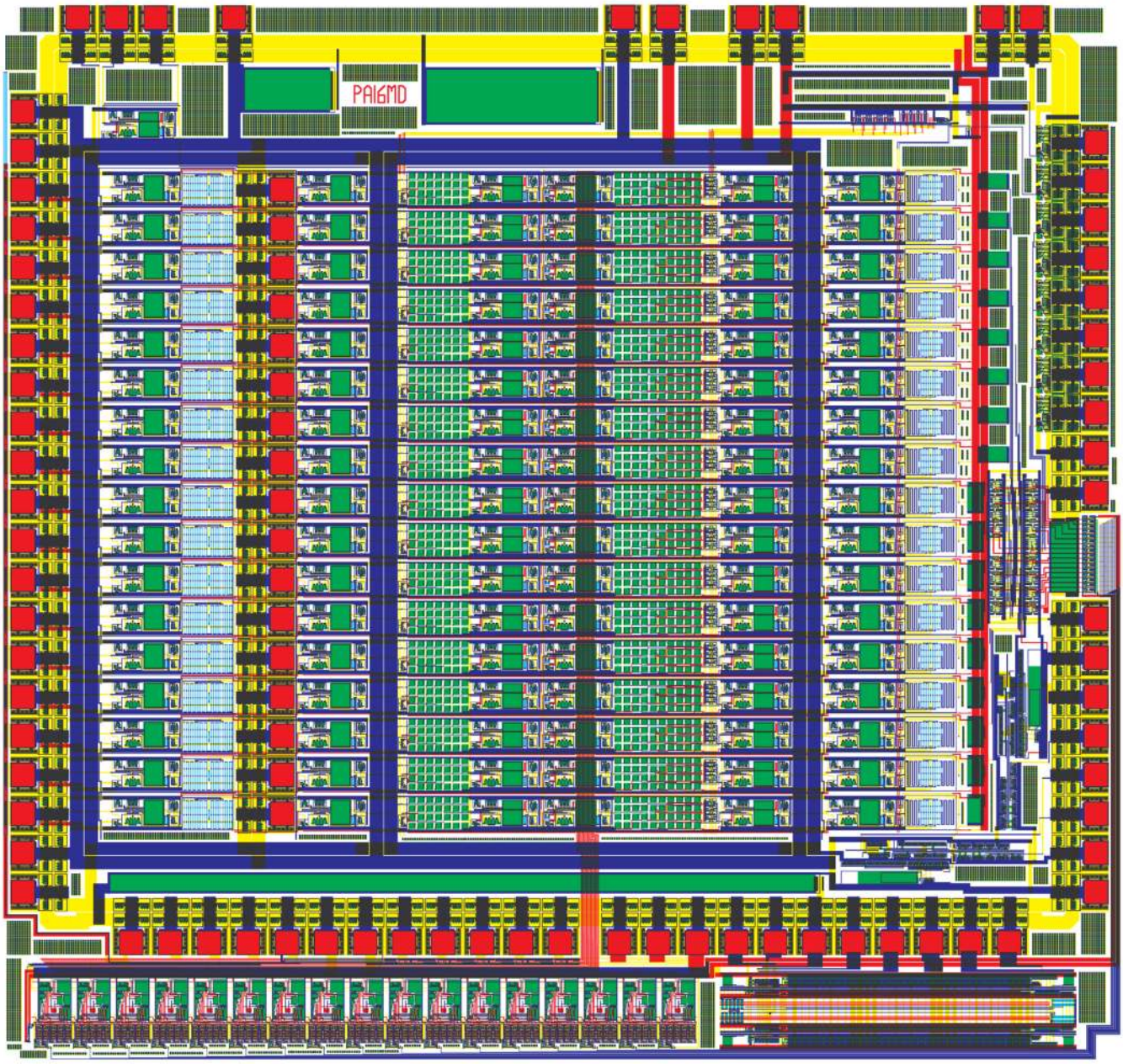

Figure 4.
Drawing of the custom integrated-circuit amplifiers. The pads that connect to the neural probes are along the left edge. The amplifiers for each channel are in the repeating horizontal pattern that spans almost the entire chip. The digital-to-analog converters are in the lower left. The differential amplifier is in the lower right.

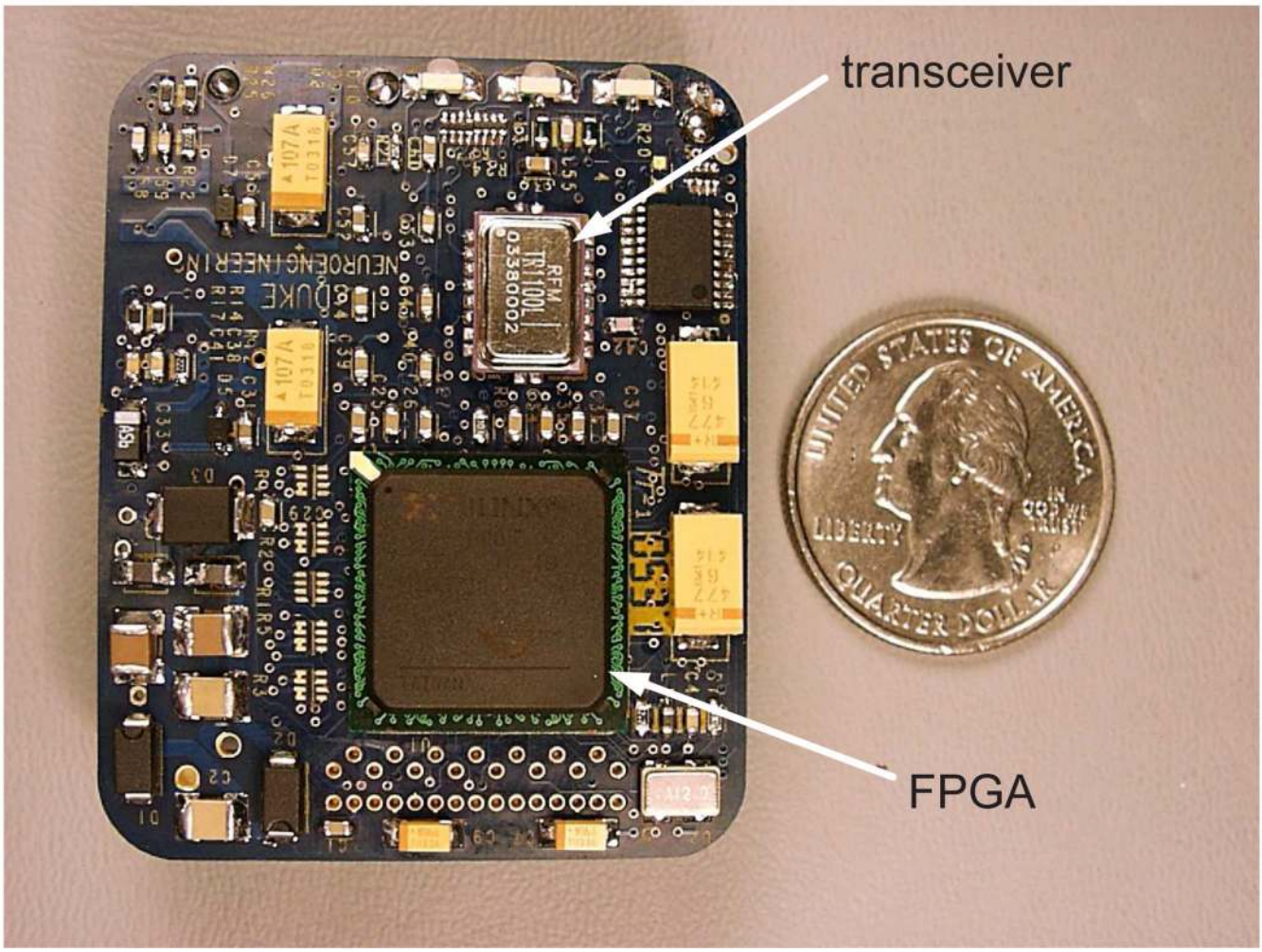

Figure 5.
The implantable central communications module (ICCM) circuit board. The arrows indicate the neural signal processor FPGA and the transceiver. An identical board is used for the wireless communications module (WCM). Figure used with permission from [12].

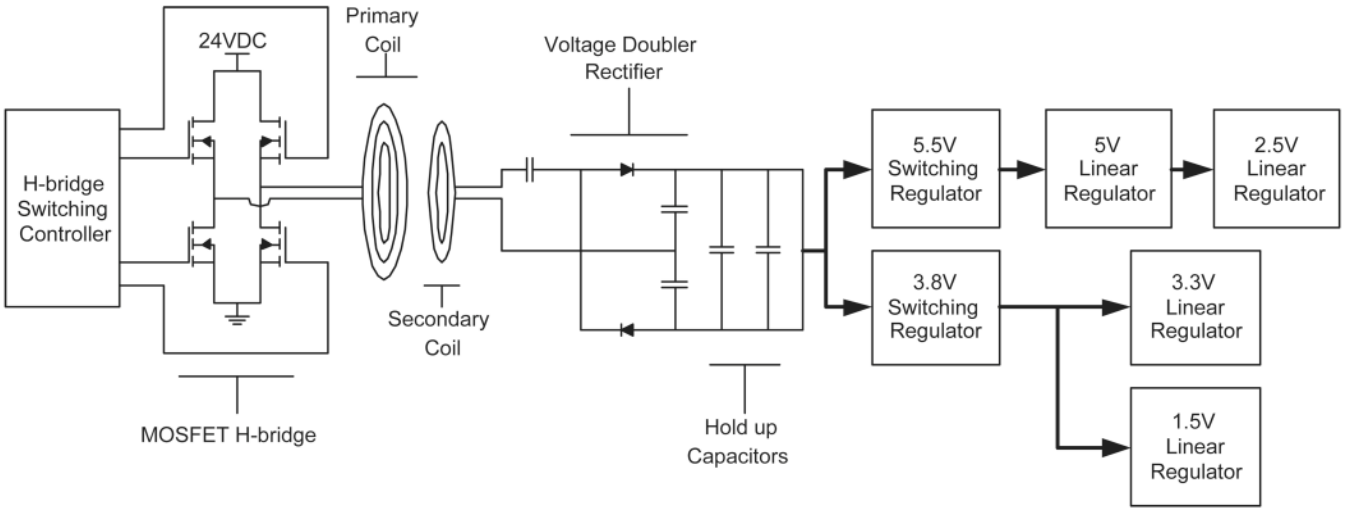

Figure 6.

Diagram of the transcutaneous energy transfer system (TETS) used to power the implanted system. A commercially available H-bridge controller switches on anti-parallel pairs of MOSFETs in the H-bridge inverter. The externally worn primary coil energizes the implanted secondary coil through linked magnetic flux. The step-up winding scheme and voltage doubler rectifier ensure that the input voltage to the switching regulators is well above the dropout voltage.

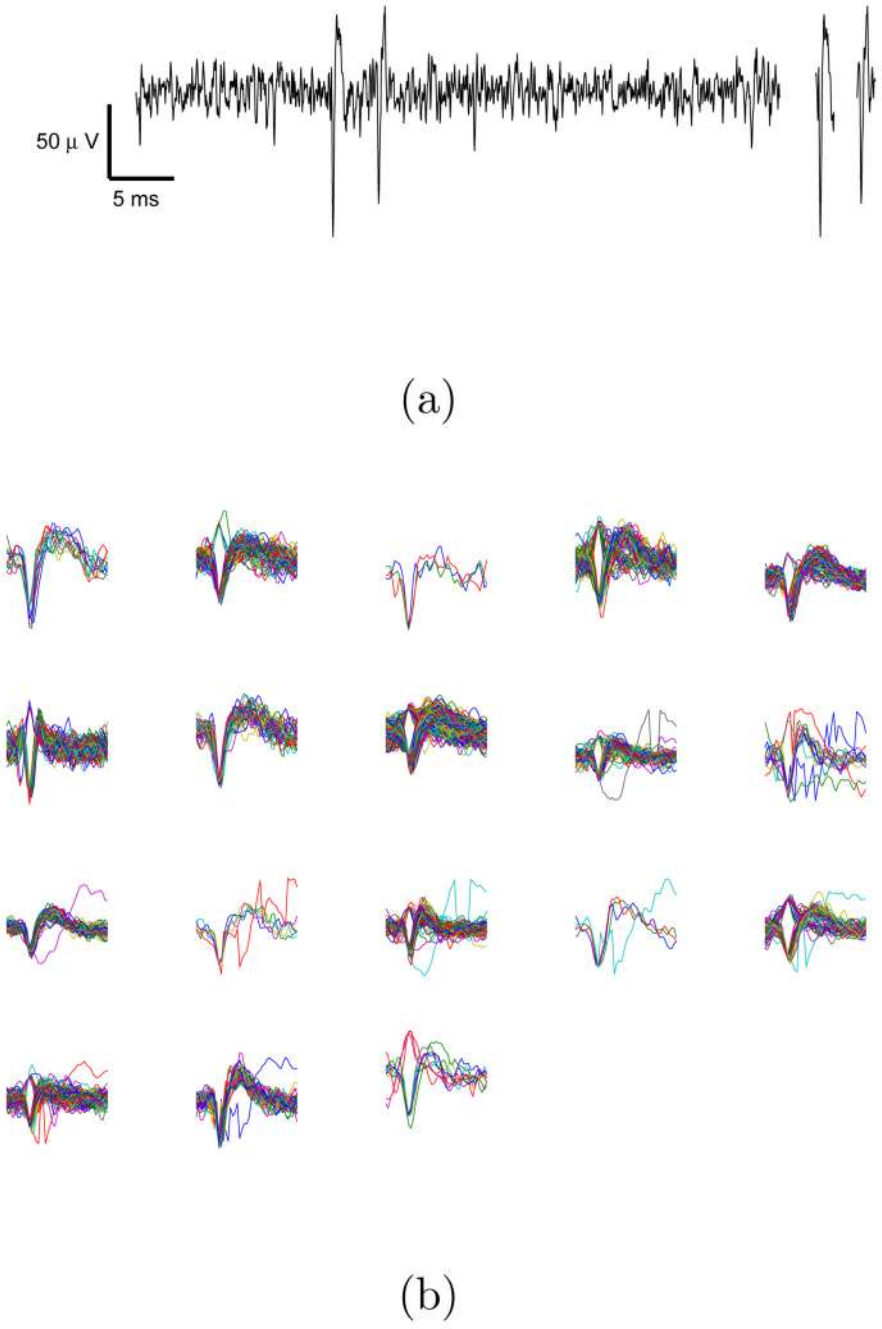

Figure 7.
Neural data recorded percutaneously from an owl monkey. (a) Fifty milliseconds of streaming data from a single channel. At the right are the two spike waveforms extracted by our system. (b) Spikes extracted by our system from several channels over a roughly one-minute period.

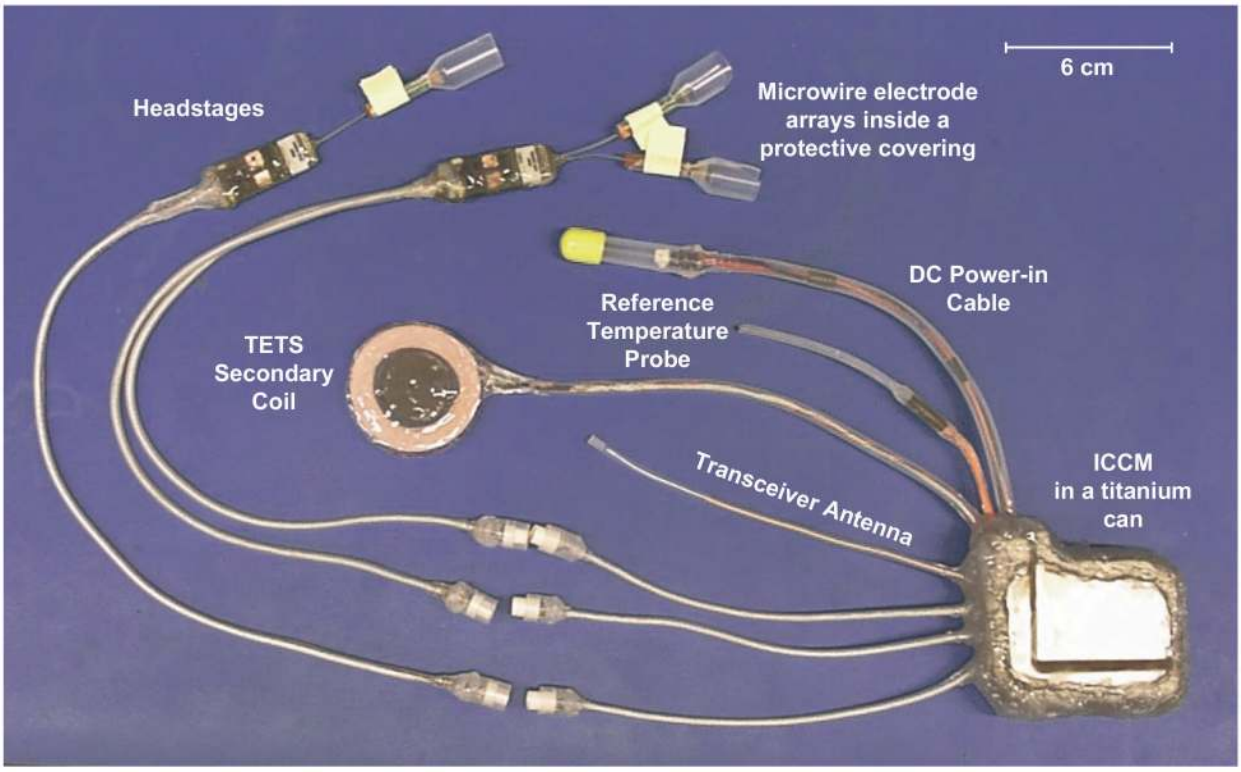

Figure 8.
The implantable portions of the neural data acquisition system packaged for implantation. The reference temperature probe and the DC power-in cable were used for evaluation purposes and are not required for the system to be functional. The system shown here was implanted in a sheep.

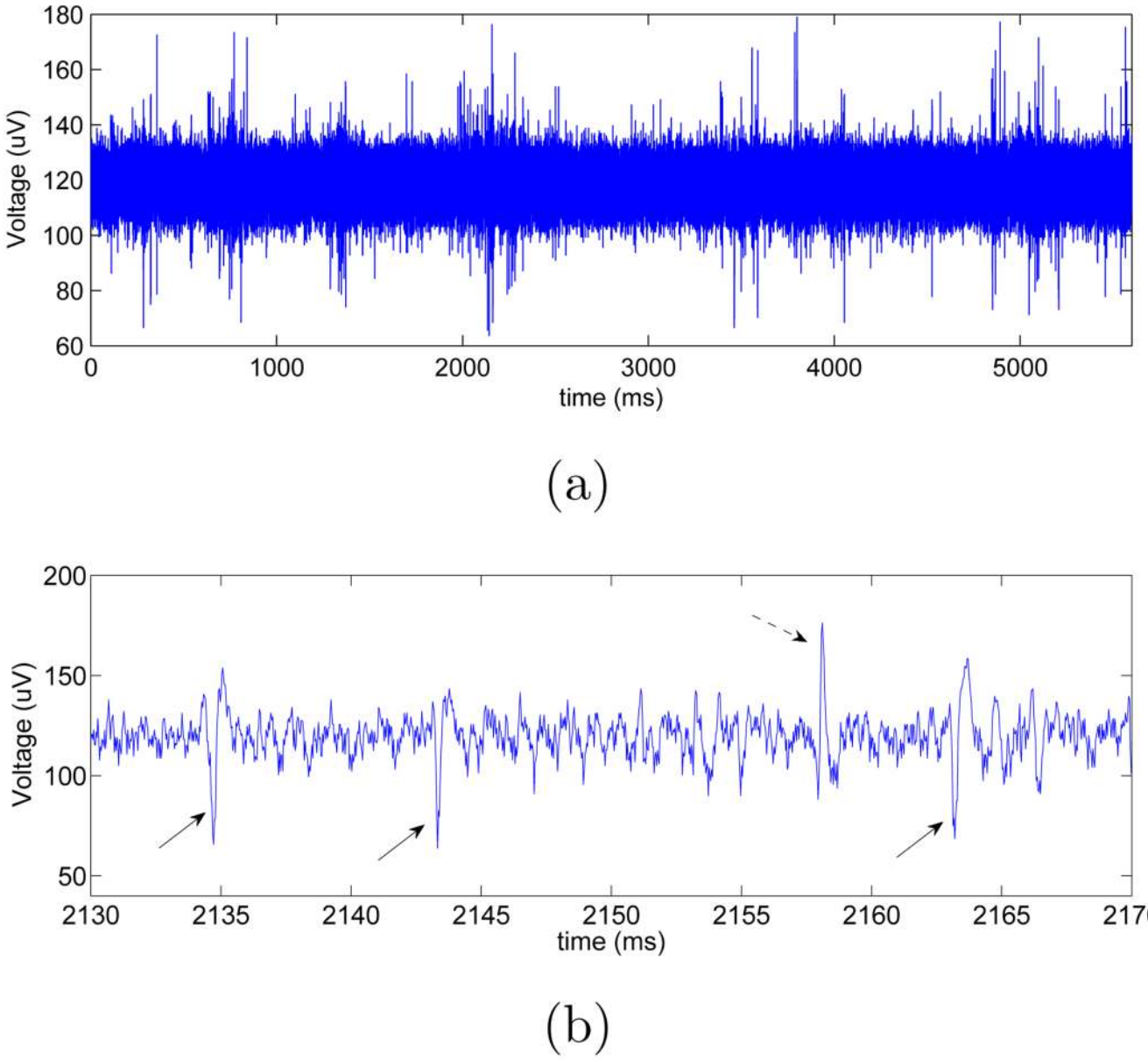

Figure 9.

(a) Streaming neural data recorded by our system while it was fully implanted in a sheep. (b) A zoomed-in portion of some of the data. The three solid arrows point to spikes that presumably came from a neuron near this particular channel's electrode. The dashed arrow points to a spike that presumably came from a neuron near the reference electrode.

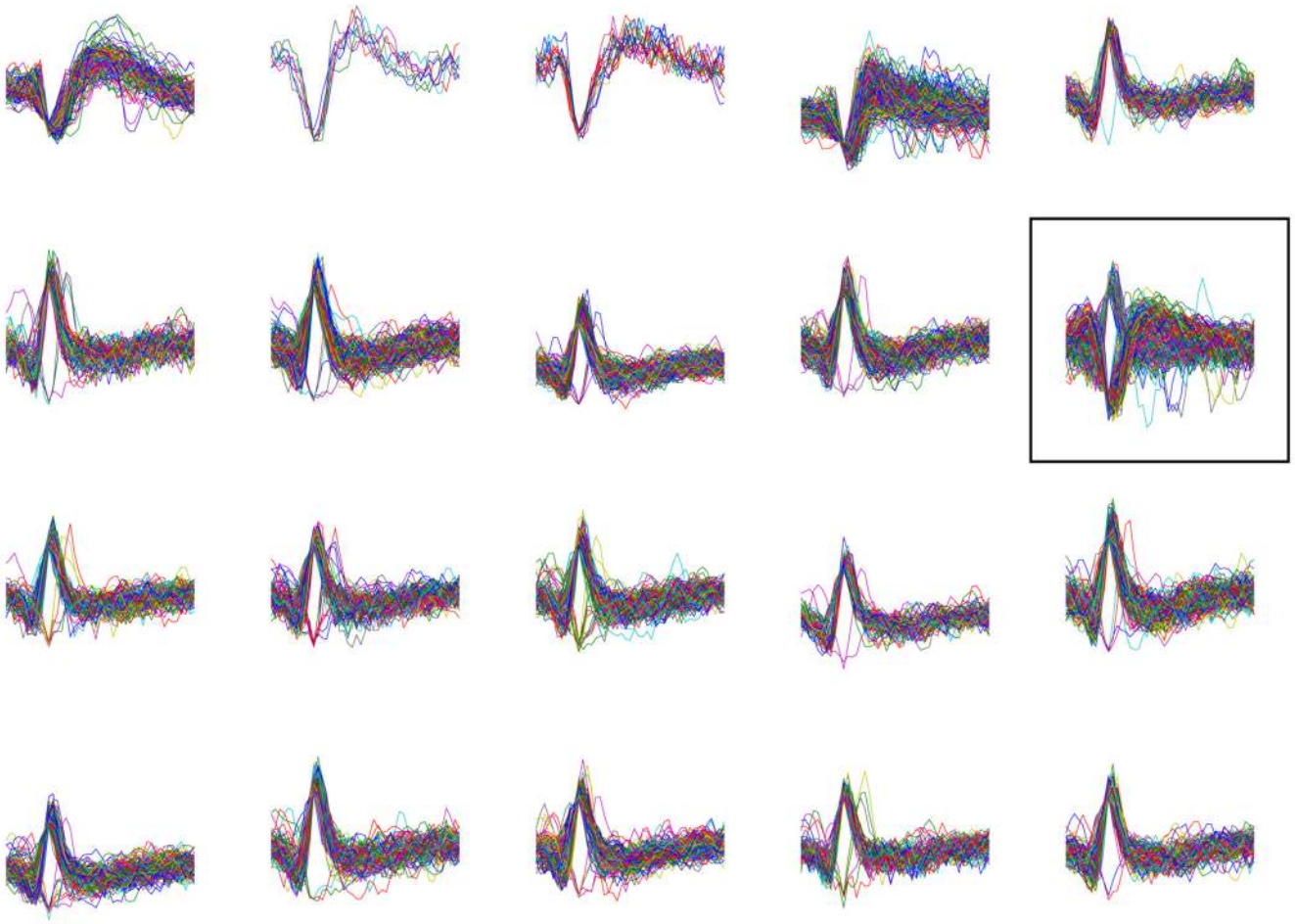

Figure 10.

Spikes extracted from several channels while the system was fully implanted in a sheep. These spikes were extracted by our system from selected channels over a roughly one-minute period. Extractions occurring on the positive threshold have been removed for the first 4 channels. For the remaining channels, all spikes extracted by the system are shown. These last 16 channels all shared a common reference electrode, and the majority of extractions are presumably due to neural activity near the reference electrode. For the boxed channel, spikes were extracted due to activity near the reference electrode and due to activity near the channel's electrode. The boxed channel is the channel for which streaming data is shown in figure 9.

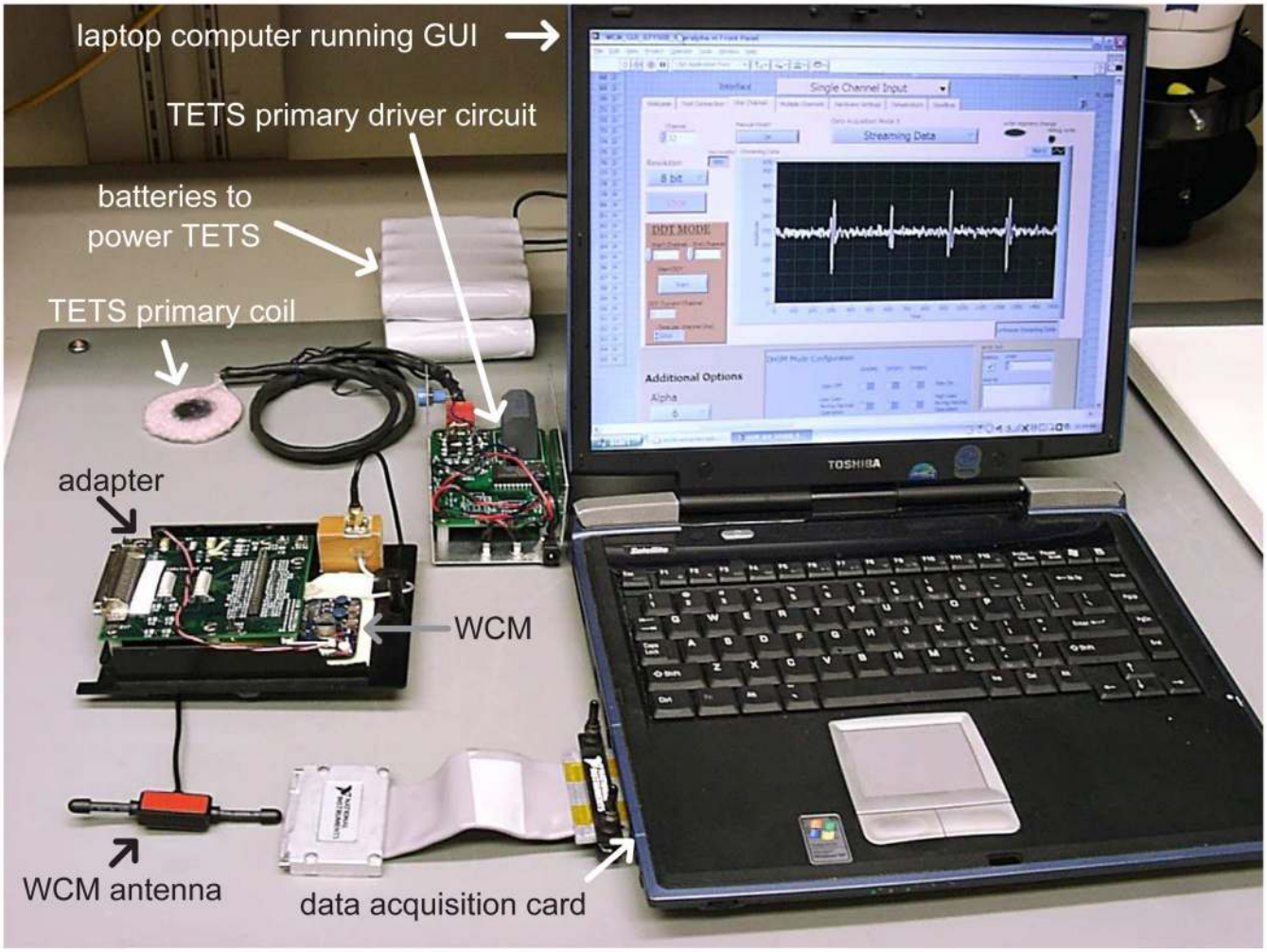

Figure 11.
The external components of the neural data acquisition system. The adapter allows the WCM to plug into the data acquisition card installed in the laptop computer.

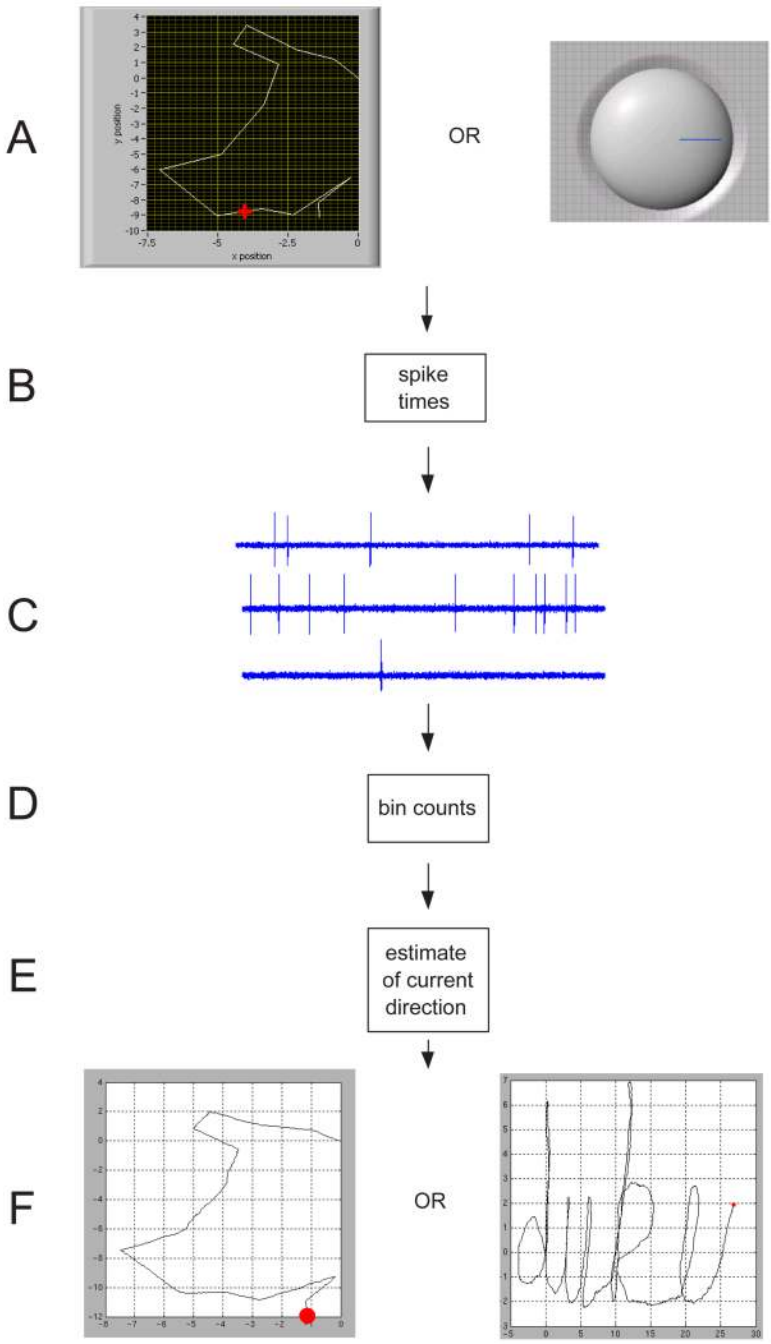

Figure 12.

Flow of information in the BMI setup. (A) Current direction of motion is determined based on either the predetermined trajectory or the "joystick" input. (B) Instantaneous firing rates are computed based on tuning curves and then spike times are generated. (C) Analog waveforms are constructed based on the spike times and then sent to the neural data acquisition system. (D) The neural data acquisition system performs spike detection (and possibly spike sorting) and outputs 50-ms bin counts. (E) The bin counts are sent to a decoder that maps the bin counts to a direction in real time. (F) The estimated trajectory is updated in real time based on the estimate of the current direction. The reconstructed trajectory on the left in (F) can be seen to match the predetermined (i.e., true) trajectory on the left in (A) quite well. For real-time

estimation of a joystick-controlled trajectory, fairly good control of the estimated trajectory (seen on the right in (F)) can be achieved. Our ability to write “duke” is evidence of this. The joystick is seen on the right in (A).

Table 1

Implanted telemetry results for two sheep.

distance between antennas	antenna orientation (0° =parallel)	total number of packets received	number of Loopback packets with errors	number of packets that were dropped	notes
0.5 m	45°	111787	0	16	*a,b*
1.5 m	0°	2162	0	3	*a*
1.5 m	45°	2165	0	1	*a*
1.5 m	90°	2794	4	3	*a*
1.2 m	0°	15992	0	1	*c*
2.2 m	*d*	9372	139	11	*c*
2.2 m	*d*	2664	145	8	*c*

a implanted antenna was a dipole made of stranded stainless steel wire

b this represents approximately 1.5 hours of data collection

c implanted antenna was a monopole made from coaxial cable and was implanted 4 mm deep

d in these cases, the antennas were oriented such that the axis of neither antenna was perpendicular to the line between the two antennas